PSFC/JA-21-38

Burning plasma achieved in inertial fusion

A.B. Zylstra[1,*], O.A. Hurricane[1,*], D.A. Callahan[1], A.L. Kritcher[1], J. Ralph[1], H.F. Robey[2], J.S. Ross[1], C. Young[1], K. Baker[1], D. Casey[1], T. Do¨ppner[1], L. Divol[1], M. Hohenberger[1], S. Le Pape[7], A. Pak[1], P. Patel[1], R. Tommasini[1], S. Ali[1], B. Bachmann[1], R. Benedetti[1], D. Berger[1], R. Betti[3], S. Bhandarkar[1], R. Bionta[1], N. Birge[2], E. Bond[1], D. Bradley[1], T. Braun[1], T. Briggs[1], M. Bruhn[1], H. Chen[1], P. Celliers[1], T. Chapman[1], C. Choate[1], A. Christopherson[1], D. Clark[1], E. Dewald[1], J.-M. Di Nicola[1], T. Dittrich[1], M.J. Edwards[1], M. Farrell[4], J. Field[1], D. Fittinghoff[1], J. Frenje[6], J. Gaffney[1], G. Grim[1], S. Haan[1], K. Hahn[1], G. Hall[1], J. Hammer[1], E. Hartouni[1], J. Heebner[1], V. Hernandez[1], H. Herrmann[2], M. Herrmann[1], D. Hinkel[1], J. Holder[1], L. B. Hopkins[1], W. Hsing[1], K. Humbird[1], N. Izumi[1], J. Jeet[1], M. Gatu Johnson[6], O. Jones[1], S. Kerr[1], S. Khan[1], J. Kilkenny[4], Y. Kim[2], H. Geppert Kleinrath[2], V. Geppert Kleinrath[2], J. Kline[2], J. Kroll[1], C. Kong[4], O.L. Landen[1], D. Larson[1], N.C. Lemos[1], J. Lindl[1], A. Mackinnon[1], B. MacGowan[1], S. Maclaren[1], A. MacPhee[1], D. Mariscal[1], E. Marley[1], L. Masse[1], K. Meaney[2], N. Meezan[1], P. Michel[1], M. Millot[1], J. Milovich[1], J. Moody[1], A. Moore[1], K. Newman[1], A. Nikroo[1], R. Nora[1], L. Pelz[1], L. Peterson[1], N. Rice[4], H. Rinderknecht[3], M. Rosen[1], M. Rubery[8], J. Salmonson[1], J. Sater[1], D. Schlossberg[1], M. Schneider[1], K. Sequoia[4], S. Shin[1], V. Smalyuk[1], B. Spears[1], P. Springer[1], M. Stadermann[1], S. Stoupin[1], D. Strozzi[1], C. Thomas[3], E. Tubman[1], R. Town[1], C. Weber[1], K. Widmann[1], C. Wild[5], C. Wilde[2], T. Woods[1], B. Woodworth[1], B. Van Wonterghem[1], P. Volegov[2], and S. Yang[1],

[1] Lawrence Livermore National Laboratory, Livermore, California 94551, USA
[2] Los Alamos National Laboratory, Los Alamos, NM 87545
[3] Laboratory for Laser Energetics, University of Rochester, Rochester, New York 14623, USA
[4] General Atomics, San Diego, California 92186, USA
[5] Diamond Materials Gmbh, 79108 Freiburg, Germany
[6] Massachusetts Institute of Technology, Cambridge, Massachusetts 02139, USA
[7] Laboratoire pour l'utilisation des Lasers Intenses chez Ecole Polytechnique, 91128 Palaiseau cedex, France
[8] Atomic Weapons Establishment, Aldermaston, RG7 4PR, United Kingdom

May 2021

Plasma Science and Fusion Center
Massachusetts Institute of Technology
Cambridge MA 02139 USA

This work was performed under the auspices of the U.S. Department of Energy by Lawrence Livermore National Laboratory under Contract DE-AC52-07NA27344. The MIT effort was supported by LLNL under contract number B640112 and by DOE/NNSA under contract number DE-NA0003868.

Submitted to *Nature - International Weekly Journal of Science*

Burning plasma achieved in inertial fusion

A.B. Zylstra[1,*], O.A. Hurricane[1,*], D.A. Callahan[1], A.L. Kritcher[1], J. Ralph[1], H.F. Robey[2], J.S. Ross[1], C. Young[1], K. Baker[1], D. Casey[1], T. Döppner[1], L. Divol[1], M. Hohenberger[1], S. Le Pape[7], A. Pak[1], P. Patel[1], R. Tommasini[1], S. Ali[1], B. Bachmann[1], R. Benedetti[1], D. Berger[1], R. Betti[3], S. Bhandarkar[1], R. Bionta[1], N. Birge[2], E. Bond[1], D. Bradley[1], T. Braun[1], T. Briggs[1], M. Bruhn[1], H. Chen[1], P. Celliers[1], T. Chapman[1], C. Choate[1], A. Christopherson[1], D. Clark[1], E. Dewald[1], J.-M. Di Nicola[1], T. Dittrich[1], M.J. Edwards[1], M. Farrell[4], J. Field[1], D. Fittinghoff[1], J. Frenje[6], J. Gaffney[1], G. Grim[1], S. Haan[1], K. Hahn[1], G. Hall[1], J. Hammer[1], E. Hartouni[1], J. Heebner[1], V. Hernandez[1], H. Herrmann[2], M. Herrmann[1], D. Hinkel[1], J. Holder[1], L. B. Hopkins[1], W. Hsing[1], K. Humbird[1], N. Izumi[1], J. Jeet[1], M. Gatu Johnson[6], O. Jones[1], S. Kerr[1], S. Khan[1], J. Kilkenny[4], Y. Kim[2], H. Geppert Kleinrath[2], V. Geppert Kleinrath[2], J. Kline[2], J. Kroll[1], C. Kong[4], O.L. Landen[1], D. Larson[1], N.C. Lemos[1], J. Lindl[1], A. Mackinnon[1], B. MacGowan[1], S. Maclaren[1], A. MacPhee[1], D. Mariscal[1], E. Marley[1], L. Masse[1], K. Meaney[2], N. Meezan[1], P. Michel[1], M. Millot[1], J. Milovich[1], J. Moody[1], A. Moore[1], K. Newman[1], A. Nikroo[1], R. Nora[1], L. Pelz[1], L. Peterson[1], N. Rice[4], H. Rinderknecht[3], M. Rosen[1], M. Rubery[8], J. Salmonson[1], J. Sater[1], D. Schlossberg[1], M. Schneider[1], K. Sequoia[4], S. Shin[1], V. Smalyuk[1], B. Spears[1], P. Springer[1], M. Stadermann[1], S. Stoupin[1], D. Strozzi[1], C. Thomas[3], E. Tubman[1], R. Town[1], C. Weber[1], K. Widmann[1], C. Wild[5], C. Wilde[2], T. Woods[1], B. Woodworth[1], B. Van Wonterghem[1], P. Volegov[2], and S. Yang[1],

[1] Lawrence Livermore National Laboratory, Livermore, California 94551, USA
[2] Los Alamos National Laboratory, Los Alamos, NM 87545
[3] Laboratory for Laser Energetics, University of Rochester, Rochester, New York 14623, USA
[4] General Atomics, San Diego, California 92186, USA
[5] Diamond Materials Gmbh, 79108 Freiburg, Germany
[6] Massachusetts Institute of Technology, Cambridge, Massachusetts 02139, USA
[7] Laboratoire pour l'utilisation des Lasers Intenses chez Ecole Polytechnique, 91128 Palaiseau cedex, France
[8] Atomic Weapons Establishment, Aldermaston, RG7 4PR, United Kingdom
[*] these authors contributed equally: A.B. Zylstra, O.A. Hurricane

The achievement of obtaining a burning plasma is a critical step toward self-sustaining fusion energy[1]. A burning plasma is a fusion plasma where the alpha-particles created by the deuterium-tritium (DT) fusion reactions are the primary source of heating in the plasma, which is necessary to sustain and propagate the fusion reaction to enable high energy gain. After decades of fusion research, a burning plasma state has finally been achieved. Herein, we report upon the first burning-plasma experiments; this state was achieved using a strategy to increase the capsule spatial-scale[2,3] via two different implosion concepts[4–7], on the US National Ignition Facility. These experiments show energies from self-heating in excess of the mechanical work injected into the implosions satisfying several burning plasma metrics[3,8], the last experiment additionally shows that the fusion self-heating is greater than losses from radiation and heat conduction. These experiments triple the fusion yield performance and show significantly higher yield amplification from self-heating than prior results; remaining degradations can be reduced for even higher fusion performance.

In order for a DT fusion [$D + T \rightarrow \alpha$(3.5 MeV)+n(14 MeV)] plasma to become thermally unstable and ignite, it must first obtain a state ('burning') where the self-heating feedback from α-particle deposition exceeds the heating input into the DT, $Q_\alpha > 1$[8]. A burning plasma state signifies a transformational change to the energy and power balance in the DT plasma, opening up the potential for rapidly increasing performance. In the impulsive case of inertial confinement fusion (ICF)[9], Q_α is a statement of energy while for the near steady-state operation of magnetic fusion energy (MFE), Q_α is a statement of power. Since α-particles carry $1/5$ of the total fusion energy per $D+T$ reaction, $Q_\alpha = Q/5$, where Q is the total fusion energy compared to the heating energy supplied (or stated in terms of fusion power over heating power in the MFE case, e.g. the goal of ITER[10] is to reach $Q \approx 10$ while the record from the JET tokamak[11] is $Q \approx 0.67$).

Burning is distinct from "igniting," which is a state that additionally requires that the self-heating from α-particles outstrips all forms of cooling in the fusing plasma, primarily the processes of Bremsstrahlung radiation, electron heat condition, and negative mechanical 'PdV' work (in the case of ICF). Therefore, no *net* energy gain, G, is expected for a burning plasma, but gain with respect to the energy that is deposited into the DT is possible (i.e. fuel-gain[12], $G_{fuel} = Y/E_{DT} > 1$, where Y is the fusion yield and E_{DT} is the total energy injected into the DT) and has already been achieved ($G_{fuel} = 1.9$ and $Q_\alpha \approx 0.38$)[13] and exceeded ($G_{fuel} = 4.5$ and $Q_\alpha \approx 0.9$)[14]. While short of ignition, a burning plasma ($Q_\alpha > 1$) is a new physics regime for laboratory fusion;[1,10,15] in this regime the self-heating can begin to exceed some or all of the loss mechanisms.

In a tokamak, once the plasma discharge is generated by resistive heating, external power sources, such as radio-frequency antenna, provide additional plasma heating as the plasma is brought to fusion conditions. In ICF, the way energy is delivered to the fusion fuel is different and much less direct. On the National Ignition Facility (NIF)[16] 192 lasers deliver up to 1.9 MJ of frequency-tripled blue light into a high atomic number (Z) "hohlraum" (Fig. 1) that serves the purpose of an x-ray converter generating a nearly Planckian x-ray bath, an approach known as 'indirect drive'[17]. The incident beam-by-beam laser pointing and power in time are designed[6] to generate a specific radiation temperature (T_{rad}) history (Fig. 1, lower left) inside the hohlraum with sufficient uniformity in a way that is matched to specifics of the target geometry and desired final plasma state. The exposed surface of a capsule at the center of the hohlraum absorbs $\sim 10 - 15\%$ of the x-rays, causing the outer edge of the capsule (the ablator) to ionize, generate high pressures of order hundreds of Mbar, and expand away from the capsule – a process termed ablation. A shell of cryogenic DT fuel is

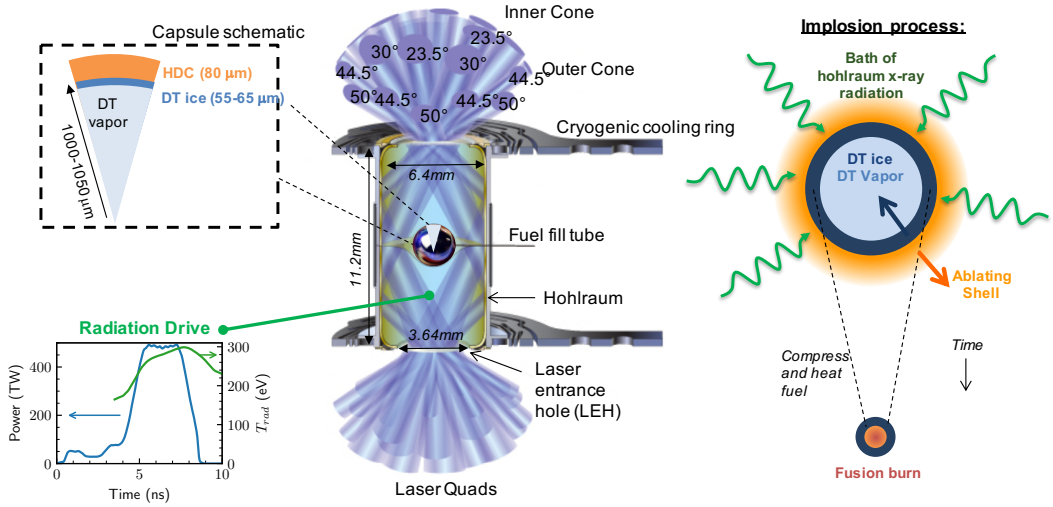

Figure 1 | (Center) A typical indirect-drive target configuration with key engineering elements labeled. Laser beams (blue) enter the hohlraum through laser entrance holes at various angles. (Upper left) A schematic pie diagram showing the radial distribution and dimensions of materials in diamond (high density carbon, HDC) ablator implosions. (Lower left) The temporal laser power pulse-shape (blue) and associated hohlraum radiation temperature (green). (Right) At the center of the hohlraum, the capsule is bathed in x-rays, which ablate the outer surface of the capsule. The pressure generated drives the capsule inward upon itself (an implosion) which compresses and heats the fusion fuel.

layered against the inside surface of the ablator, which is in partial-pressure equilibrium with DT vapor in the center of the capsule (Fig. 1 upper left). The inwardly directed acceleration caused by the ablation drives the capsule and DT fuel inwards upon itself (an implosion, shown schematically at the right of Fig. 1) with enormous acceleration ($\sim 10^{13}$ g's) obtaining velocities of $\sim 350-400$ km/s in a matter of nano-seconds. Most of the capsule ($\sim 92-95\%$) and absorbed x-ray energy is consumed by the ablation process, but as a result the DT fuel obtains significant ($\sim 10-20$ kJ) kinetic energy (KE) inside a very small volume.

Shortly after the DT fuel acquires peak KE, it has been squeezed into such a small volume that there is nowhere else to go and the pressures (P) internal to the implosion rise dramatically, to levels of many hundreds of Gbar, as KE is converted into internal energy (IE) in the DT (a process termed stagnation). By its nature, an ICF implosion is a pressure amplifier, sacrificing a great deal of absorbed energy in order to achieve high *energy density* and central pressures that are factors of thousands higher than the pressure at the ablation front. The high central pressure is necessary because only a small fraction of the NIF facility energy can ever be coupled into the DT fuel and heating a large mass of DT fuel is energetically costly, as reflected in the heat capacity of DT, $c_{DT} = 115$ MJ/(g·keV). Since high T_i is also needed for fusion, as the fuel stagnates at the center of the implosion, the DT forms a hot-spot from the fuel's inner surface and PdV work is done on the hot-spot generating very high ion and electron temperatures in near thermal equilibrium ($T_i \approx T_e \sim 4-5$ keV). If the conditions of high temperature and pressure are achieved, the hot-spot initiates copious DT fusion reactions and self-heating further increases T_i.

ICF experiments demonstrated significant fusion performance enhancement from self-heating[13,18] several years ago, and more recent advances[14,19,20] generated experiments with ~ 50 kJ fusion yields that were close to the burning plasma threshold[3]. Within the maximum laser energy NIF can deliver, these previous designs were limited in the energy coupled to the capsule and fuel kinetic energy by the ability to control the symmetry of the radiation environment within the hohlraum, primarily due to the fact that an expanding of ablated plasma expands from where the outer beams hit the wall (see Fig. 1) and intercepts the inner beams, suppressing drive at the hohlraum waist[21]. Two tactics have been developed to enable symmetry control with more efficient hohlraums: employing cross-beam energy transfer to transfer energy from the outer to inner beams[4,22], and incorporating a pocket in the hohlraum wall at the outer beam location to delay the bubble propagation[5]. These innovative tactics have been used to design higher efficiency hohlraums that can maintain symmetry control; we use these hohlraums to drive capsules that are $\sim 10\%$ larger than prior experiments to realize the strategy for achieving a burning plasma laid out in Ref. 2. Development details for the symmetry control tactics and higher efficiency hohlraums are given in the accompanying Letters[6,7] describing these campaigns, known as 'Hybrid E' (HyE) and 'I-Raum'. The HyE campaign uses cross-beam energy exclusively while I-Raum uses a combination of the pocket described above and cross-beam energy transfer.

Three experiments with these new designs have been conducted that have generated record performance on the NIF, with fusion yield tripled from past experiments[4,14,20] to a maximum ~ 170 kJ; the experiments are referred to by a shot number denoting the date of the experiment (N201101, N201122, and N210207; in NYYMMDD, YY=year, MM=month, DD=day format). N201101 and N210207 were experiments using the HyE platform while N201122 and N210220 were shots I-Raum platform. Key data are shown in Table 1: the total fusion yield in kJ, ion temperature (T_i), hot-spot volume, and burn width in ps. For a full description of the shot data and changes between the shots, see Ref. 7. From these data analytic models are used to infer characteristics of the implosion process and hot spot including the pressure, hot-spot internal energy, implosion velocity and peak kinetic energy in the fuel during implosion, PdV work done on the hot spot, and areal density of the hot spot in g/cm^2. These quantities are required to evaluate the burning-plasma criteria. Most of these inferences are described in Ref. 23 and the Methods; the implosion velocity (v_{imp}) can be inferred from the time of maximum neutron output ('bang-time') and an implosion dynamics 'rocket-model' that is calibrated to near-neighbor surrogate experiments where the implosion trajectory is tracked radiographically[24,25].

G_{fuel} has a direct connection to ignited fusion requirements and suggests a simple metric for assessing a burning plasma. Since, from the total fusion yield produced by a mass (m) of DT, over a character-

Table 1 | Data, inferred metrics, and burning-plasma criteria for these four experiments. Percentages indicate probabilities. Error bars formal $\pm 1\sigma$ standard deviations.

		N201101 (HyE)	N201122 (I-Raum)	N210207 (HyE)	N210220 (I-Raum)
Data	Yield (kJ)	98.4 ± 2.7	106.2 ± 3.2	170.9 ± 4.8	160.6 ± 4.3
	T_i (keV)	4.61 ± 0.14	4.65 ± 0.14	5.23 ± 0.16	5.13 ± 0.24
	Volume ($10^5 \mu m^3$)	2.5 ± 0.1	2.5 ± 0.1	3.2 ± 0.1	2.5 ± 0.1
	Burn Width (ps)	130 ± 20	139 ± 12	107 ± 13	136 ± 13
Inferred	Pressure (GBar)	312^{+37}_{-29}	295^{+21}_{-19}	338^{+27}_{-23}	351^{+50}_{-42}
	Hot-spot energy (kJ)	$11.9^{+1.4}_{-1.1}$	$11.3^{+0.8}_{-0.7}$	$16.9^{+1.3}_{-1.1}$	$13.1^{+1.7}_{-1.5}$
	Fuel K.E. (kJ)	15.9 ± 1.0	11.6 ± 0.87	15.9 ± 1.0	11.6 ± 0.7
	PdV work (kJ, exp.)	9.5 ± 0.8	8.6 ± 0.7	10.6 ± 0.9	8.5 ± 1.4
	PdV work (kJ, sim.)	10.1 ± 0.5	10.1 ± 0.5	11 ± 0.5	10.5 ± 0.5
	Hot-spot ρR (g/cm^2)	$0.36^{+0.05}_{-0.04}$	$0.33^{+0.04}_{-0.03}$	$0.36^{+0.04}_{-0.03}$	$0.36^{+0.04}_{-0.04}$
Criteria	Y_{amp}	3.5 ± 0.2	4.2 ± 0.2	4.7 ± 0.3	5.7 ± 0.5
	G_{fuel}	$5.9^{+0.3}_{-0.4}$ (99%)	$6.8^{+0.5}_{-0.8}$ (100%)	$7.8^{+0.7}_{-1.0}$ (100%)	$10.7^{+2.0}_{-2.4}$ (100%)
	E_α/KE	1.28 ± 0.09 (100%)	1.79 ± 0.13 (100%)	2.13 ± 0.15 (100%)	2.72 ± 0.19 (100%)
	v_{cond}/v_{imp} (Hurricane)	1.14 ± 0.13 (86%)	1.14 ± 0.08 (98%)	1.66 ± 0.15 (100%)	1.52 ± 0.13 (100%)
	$0.5E_\alpha/E_{PdV}$ (Betti, exp.)	1.07 ± 0.09 (77%)	1.21 ± 0.10 (99%)	1.58 ± 0.14 (100%)	1.87 ± 0.31 (100%)
	$0.5E_\alpha/E_{PdV}$ (Betti, sim.)	1.01 ± 0.06 (54%)	1.03 ± 0.06 (67%)	1.49 ± 0.08 (100%)	1.50 ± 0.09 (100%)
Power (TW)	$f_\alpha m P_\alpha$	126^{+31}_{-22}	117^{+14}_{-12}	241^{+40}_{-32}	181^{+23}_{-20}
	$m f_b P_b$	159^{+49}_{-34}	135^{+29}_{-23}	190^{+41}_{-32}	165^{+34}_{-27}
	$m P_e$	19^{+4}_{-3}	21^{+4}_{-4}	36^{+6}_{-6}	27^{+6}_{-5}
	Prob. $f_\alpha P_\alpha > P_b + P_e$	0%	0%	82%	20%

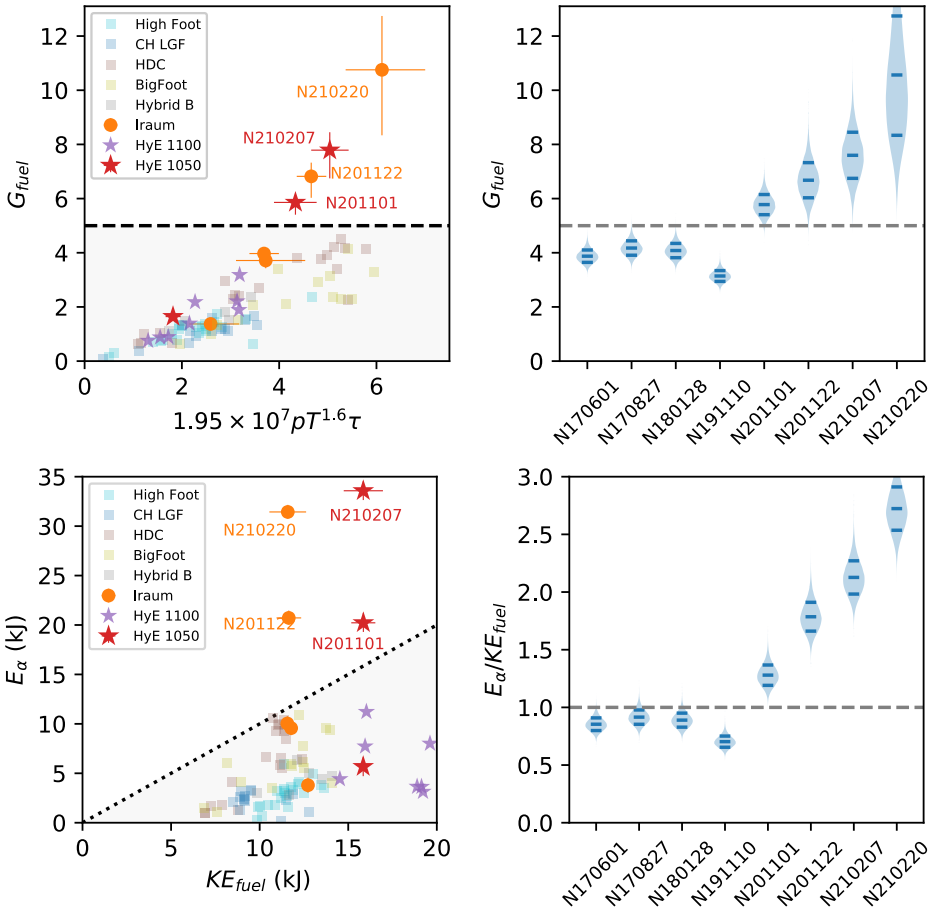

Figure 2 | Simple metrics for assessing a burning plasma. (a) total fuel gain versus Lawson-like parameter, $G_{fuel} > 5$ corresponds to the burning plasma regime. (b) Probability distributions for G_{fuel} for high-performing shots, in these plots the width of the shaded region is proportional to the probability distribution and the solid lines mark the 16, 50, and 84 percentile of the distribution (c) Total alpha-heating energy vs fuel kinetic energy, $E_\alpha/KE > 1$ corresponds to $Q_\alpha > 1$. (d) Probability distributions in E_α/KE criteria for high performing shots

istic confinement-time, τ, is $Y \sim 5 m P_\alpha \tau$ ($P_\alpha = 8.2 \times 10^{24} \rho \langle \sigma v \rangle$ in GJ/(g·s) being the specific DT fusion power for a given mass density, ρ, of DT with reaction-rate $\langle \sigma v \rangle$) and since the internal energy in that

DT is $E_{hs} = c_{DT} m T_i$, one can write[26]

$$G_{fuel} = \frac{Y}{E_{PdV,tot}} \approx \frac{\frac{Y}{E_{hs}}}{1 + \frac{E_{fuel}}{E_{hs}} - \frac{q}{10}\frac{Y}{E_{hs}}} \quad (1)$$

$$\text{with } \frac{Y}{E_{hs}} \approx 4.6 \times 10^{26} P \frac{\langle \sigma v \rangle}{T^2} \tau \quad (2)$$

where P is in Gbars, T_i in keV, and τ in s units. In Eq. 1, the total energy delivered by PdV work, $E_{PdV,tot}$, is determined from the hot-spot and compressed, but cold, DT fuel energy at stagnation, E_{hs} and E_{fuel} respectively. The last term in the denominator represents a correction for additional energy retained by self-heating of the fuel but not then lost as bremsstrahlung. So, $E_{PdV} \approx E_{hs} + E_{fuel} - qY/10$, where q is a "quality" factor, $0 \leq q \leq 1$, measuring the ability of the implosion to retain self-heating energy. Here we use $q \sim 0.7$, inferred from simulations. Albeit generally arrived at in a different fashion than above, the product $p(\langle \sigma v \rangle / T^2)\tau$ is Lawson's [27] parameter for ignition.

Motivated by Eqs. 1 and 2, Fig. 2a (also see Table 1) shows a plot of G_{fuel} data from many DT implosions on NIF (see Methods), using the useful reaction-rate approximation $\langle \sigma v \rangle \approx 4.2 \times 10^{-20} T_i^{3.6}$ (in units of cm^3/s for ion temperature range $3.5 < T_i < 6.5$ keV) to simplify the abscissa. As can be seen in Fig. 2a, most shot series show a linear trend between G_{fuel} and $PT_i^{1.6}\tau$ and have $G_{fuel} \leq 5$. Whereas, the Hybrid-E 1050 and I-Raum implosion series show a transition to a super-linear trend between G_{fuel} and $PT_i^{1.6}\tau$ (as expected from Eq. 1 when self-heating exceeds the hot-spot internal energy) and have $G_{fuel} > 5$. The non-burning plasma regime in denoted by the gray shaded region ($G_{fuel} < 5$).

Fig. 2b shows the probable distribution of the G_{fuel} values plotted in Fig. 2a, with the probability distribution in the inferred data quantities included to evaluate the uncertainty (see Methods). For comparison, we include a set of previous high-performing NIF experiments from Refs. 4, 14, 20. The abscissa of Fig. 2b are NIF experiment ("shot") numbers; while several experiments in years prior to November 2020 came very close to the threshold of $G_{fuel} = 5$, only the experiments reported here have so far clearly surpassed it (see Table 1 for values).

Another suggested simple metric for an ICF burning plasma is to compare the total energy produced in α-particles, $E_\alpha = Y/5$, to the peak DT fuel KE (see Fig. 2c). Similar to Fig. 2b, Fig. 2d shows the probable range of E_α/KE_{fuel}, with normally distributed uncertainties in the input data vs. shot number for the six highest performing DT experiments on the NIF, where again only these three shots clearly exceed $E_\alpha/KE_{fuel} > 1$ (see Table 1 for values).

While G_{fuel} and E_α/KE are suggestive metrics for an ICF burning plasma, two more rigorous and more difficult to satisfy metrics already exist in the literature[3,8]. First, it is important to recognize that the burning plasma statement that "α-deposition is the dominant source of plasma heating" is complicated by the temporal nature of an implosion, where the PdV work on the hot-spot that does the heating comes before the time of peak fusion-rate, a consideration that is not analogous to MFE. At the time of peak burn, the time-rate of change of hot-spot volume, dV/dt, and therefore the heating-rate is nearly zero, so time integration is needed. Mathematically, a statement of a burning plasma appropriate for ICF is

$$\int_0^{t_m} f_\alpha P_\alpha dt > -\int_0^{t_m} \frac{P}{m} dV. \quad (3)$$

where t_m is the time of minimum hot-spot volume and f_α is the fraction of α-particles that are stopped in the hot-spot[28].

The integrals in Eq. 3 can be rather easily approximated[2] without knowing the details of the actual implosion using the mathematical method of Steepest Descent. The key assumption needed is that for an implosion the thermodynamic quantities of interest, such as $T, P, \rho, \cdots$, are impulsive, being highly peaked around the time of stagnation.

The solution to Eq. 3, in terms of only burn-average hot-spot areal density, ρR_{hs}, T_i, and v_{imp} is the condition published by Hurricane[2,3]

$$v_{cond}(\rho R_{hs}, T_i) = 7.4 \times 10^{25} f_\alpha (\rho R)_{hs} \frac{\langle \sigma v \rangle}{T_i} > v_{imp} \quad (4)$$

in units of keV, g, cm, and s.

To evaluate the Hurricane metric we need to know the hot-spot temperature and areal density, and the implosion velocity. The alpha stopping fraction f_α and thermonuclear reactivity $\langle \sigma v \rangle$ are simple functions of the hot spot conditions, specifically the density and temperature; fits for f_α using modern stopping-power theory have been published[28], for the reactivity we use the fit from Bosch and Hale [29]. The implosion velocity is inferred following the prescription described earlier. Fig. 3a shows the shots in hot-spot temperature and areal density parameter space. Previous shots are shown as points, while these two experiments are shown as full probability distributions [red (N201101), blue (N201122), purple (N210207), and grey (N210220)], with contours enclosing 80% of the distribution. The Hurricane criteria is velocity dependent, a single contour of this criteria for $v_{imp} = 385$ km/s, representative of these shots, is shown. When evaluating the criteria each shot's actual inferred velocity, with uncertainty, is used. These are the first shots to exceed the Hurricane criterion, as clearly shown by the probability distributions in Fig. 3b. The likelihood of these three experiments exceeding the criteria is 86% (N201102), 98% (N201122), and 100% for both N210207 and N210220.

Eq. 4 should be roughly equivalent to the burning-plasma criteria found by Betti, *et al.* ($3.5\times$ yield amplification and $0.5E_\alpha/E_{PdV} > 1$)[8], but for completeness we use both. The first criteria by Betti *et al.*, $Y_{amp} \geq 3.5$, is satisfied by our inferred yield amplifications given in Table 1, inferred with the prescription in Ref. 23. Two quantities are required to evaluate the second Betti *et al.* burning-plasma metric. The alpha deposited energy (E_α) is straightforward as it is simply 20% of the measured total fusion yield (given in Table 1), which is ~ 20 kJ for the first two experiments, ~ 33 kJ for N210207, and ~ 31 kJ for N210220. The second input for this criteria is the PdV work done upon the hot spot, which must be inferred; these inferences are prone to large uncertainties in the presence of significant α-heating and bremsstrahlung x-ray losses. We perform this inference two ways (see Methods), first using an analytic hydrodynamic piston model[39] of an implosion, and second by extracting PdV work from the 2-D radiation-hydrodynamics simulations that best match the experimental observables as described in Ref. 6. These two estimates are both used to estimate a range in hot-spot PdV work and are both plotted in Fig. 3c compared to previous experiments on the NIF, with a $1-1$ line to denote the burning plasma regime (above the line). Probability distributions for the metric quantity itself are shown in Fig. 3d. From Betti's criteria, with the experimental (simulated) $E_{PdV,hs}$ we asses 77% (54%) and 99% (67%) probability, shots N201101 and N201122, respectively, are in the burning plasma regime. Shots N210207 and N210220 are assessed to be in the burning plasma regime with 100% confidence by both methodologies, with an inferred $Q_\alpha \geq 1.5$.

Several metrics for assessing whether these implosions created a burning plasma state have been discussed and presented in Table 1 and Figures 2 and 3. In each case burning plasma likelihoods are calculated by propagating uncertainties in each quantity through the metric (see Methods), shown in the figures with likelihood values discussed and summarized in Table 1. Quantitatively, we see that the first two (N201101 and N201122) are assessed as likely being in the burning plasma regime; the most recent shots (N210207 and N210220) are overwhelmingly likely to have passed this threshold. Qualitatively, our

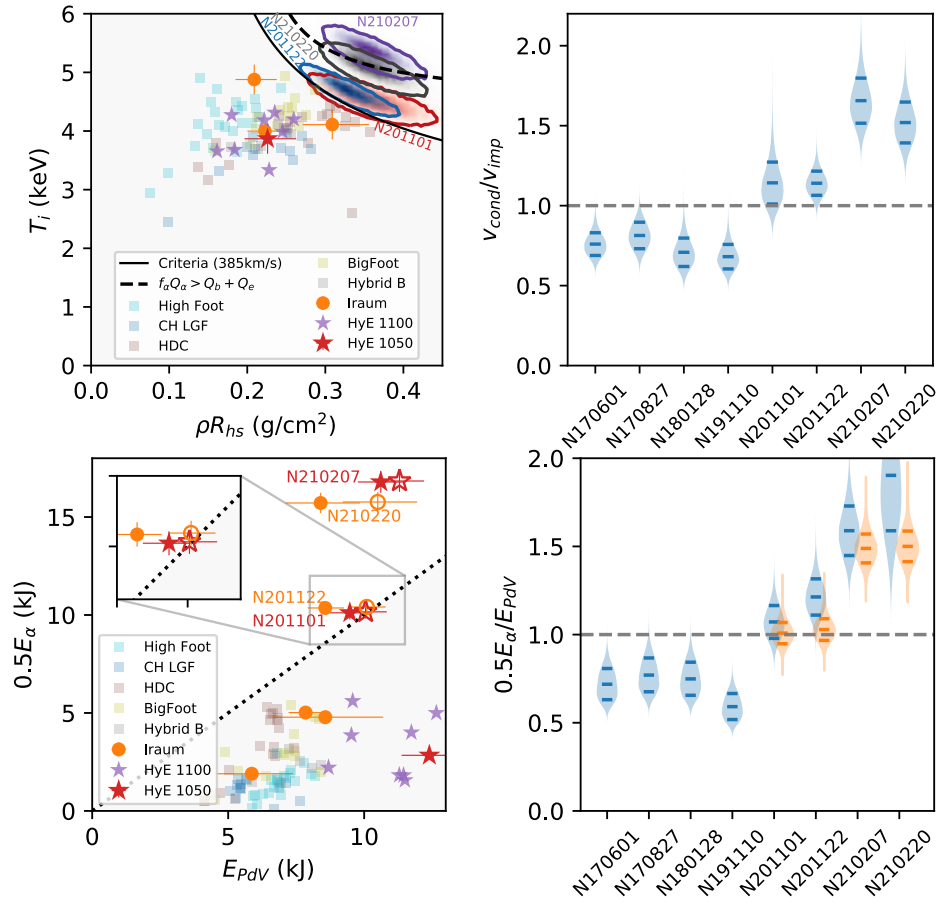

Figure 3 | ICF-specific burning plasma metrics. (a) Criteria on temperature and hot-spot ρR established by Hurricane et al. (Ref. 3) (b) probability distribution for shots exceeding the Hurricane criteria, > 1 is a burning plasma. (c) Criteria on alpha heating and PdV work from Betti et al. (Ref. 8), including estimates from data inferences (solid symbols) and from 2-D simulations (open symbols) (d) probability distribution for shots exceeding the Betti criteria, for these shots distributions are shown for data-inferred E_{PdV} (blue) and using 2-D simulations (orange).

confidence in this conclusion is further increased by the use of multiple independent metrics.

The achievement of a burning plasma state is key progress towards the larger goal of 'ignition' and overall energy gain in inertial fusion. Note that the fusion yields here (~ 0.17 MJ) are lower than the input laser energy (~ 1.9MJ), but is nearly equal to the capsule absorbed energy giving capsule gain, $G_{capsule} \sim 0.68$. In this new burning plasma regime, it is expected that the dominant alpha heating is expected to rapidly increase with modest improvements in the implosion physics or reductions in degradation mechanisms. This is consistent with the large increase in performance seen on N210207 and N210220, which are discussed in more detail in Ref. 7. Making improvements is easier said than done, so it is unlikely that ignition will be in reach within the short term.

In this new burning plasma regime the self-heating can begin to overtake loss mechanisms, which include bremsstrahlung (radiation) losses, thermal conductivity, and negative PdV work upon expansion. The hot-spot per unit mass power balance is:

$$c_{DT}\frac{dT}{dt} = f_\alpha P_\alpha - f_b P_b - P_e - \frac{p}{m}\frac{dV}{dt}, \qquad (5)$$

which describes the temporal evolution of the temperature (T) in terms of the balance of self heating (P_α) vs bremsstrahlung (P_b) and electron conduction (P_e) losses plus PdV work. Note that hot-spot volume change, dV/dt, is generally positive during and after peak burn and therefore the pdV term becomes an energy loss term. The bremsstrahlung loss can be enhanced beyond the emission of clean DT by the presence of high-Z contamination of the DT (i.e. mix), by a fraction f_b. In Eq. 5 c_{DT} is the fuel's heat capacity and f_α is the fraction of alpha particles stopped in the hot spot[28]. Simple expressions for the power balance terms are given in the Methods and values for the four shots are given in Table 1. Here, we use a bremsstrahlung enhancement factor $f_b \sim 1.15$ which is inferred from the data[34]. The first two experiments have self-heating comparable to the radiation losses. An important new regime is when self-heating is greater than both the radiation and conduction losses ($f_\alpha P_\alpha > P_b + P_e$), a contour for this regime is shown in Fig. 3 by the black dashed line. Shot N210220 is close to entering this regime, and we infer that shot N210207 has entered this regime for the first time with 82% likelihood, this is now short of ignition because the self-must must additionally overtake the negative PdV work and other loss mechanisms.

In order to achieve ignition and high gain further progress is needed. Fig. 4 shows these experiments in the larger context of ignition, in the parameter space of hot-spot pressure and energy (left) and in yield amplification versus a Lawson-like parameter called the 'ignition threshold factor' experimentally inferred (ITFX)[17,23,30] for conditions without alpha heating ($n\alpha$, right). Fig. 4 plots this quantity as $ITFX_{n\alpha}^{0.34}$ which is approximately equivalent to $\chi_{n\alpha}$ as defined in Ref. 8. Proximity to ignition can be gauged qualitatively in terms of the product $P^2 E_{hs}$, or in terms of $ITFX_{n\alpha}$ or $\chi_{n\alpha} \sim 1$ representing

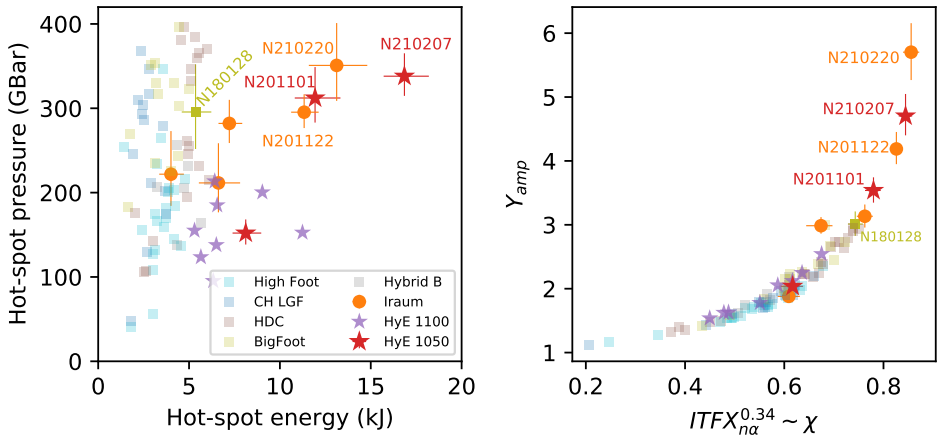

Figure 4 | These experiments in parameter space relevant for ignition. Left: Hot-spot pressure and energy, the product $P^2 E_{HS}$ is representative of proximity to ignition. Right: Yield amplification (Y_{amp}) versus $ITFX_{n\alpha}$. These shots are the highest performing ICF experiments to date and the closest to ignition.

ignition. From Fig. 4 we clearly see that these four experiments are the closest to ignition, but a further increase in $ITFX_{n\alpha}$ of $\sim 67\%$ is required.

As discussed in the accompanying Letters[6,7], these experiments have clear and specific degradation mechanisms which can be mitigated for further improvement in performance. More generally, the ICF program on NIF is pursuing several approaches that can enable additional progress: reducing degradation mechanisms including low-mode asymmetry[31–33] and radiative losses from mix[34], further increasing energy coupled to the capsule[4,35], and improving compression of the fuel[36].

In conclusion, we have generated a burning plasma state, in which the plasma is predominantly self-heated, for the first time in the laboratory. This was accomplished using inertial fusion implosions on the US National Ignition Facility; previous experiments here were just below the threshold for a burning plasma, we increase the capsule scale relative to previous work, increase the coupling efficiency from laser energy to the capsule, and control implosion symmetry using new tactics. Four experiments have been conducted that have passed the threshold for a burning plasma by several simple and inertial-fusion-specific metrics, with especially high confidence on the most recent two experiments. Additionally, the highest performing shot (N210207) is in a more stringent regime where the self-heating surpasses energy losses from radiation and conduction. While these results are short of total energy gain from the system due to the inefficiencies of converting laser energy to heating the fuel, these experiments represent a substantial step towards this goal with record values of parameters that assess our proximity to ignition on NIF. Several promising avenues for further increases in performance are identified and will be pursued by the US inertial fusion program.

1. Mauel, M. *et al. Final Report of the Committee on a Strategic Plan for U.S. Burning Plasma Research* (National Academies Press, Washington, D.C., 2019).
2. Hurricane, O. A. *et al.* Beyond alpha-heating: driving inertially confined fusion implosions toward a burning-plasma state on the National Ignition Facility. *Plasma Physics and Controlled Fusion* **61**, 014033 (2019).
3. Hurricane, O. A. *et al.* Approaching a burning plasma on the NIF. *Phys. Plasmas* **26**, 052704 (2019).
4. Zylstra, A. B. *et al.* Record Energetics for an Inertial Fusion Implosion at NIF. *Phys. Rev. Lett.* **126**, 025001 (2021).
5. Robey, H. F., Berzak Hopkins, L., Milovich, J. L. & Meezan, N. B. The I-Raum: A new shaped hohlraum for improved inner beam propagation in indirectly-driven ICF implosions on the National Ignition Facility. *Phys. Plasmas* **25**, 012711 (2018).
6. Kritcher, A., Young, C., Robey, H. *et al. Nature Physics* (2021).
7. Ross, J. S., Ralph, J., Zylstra, A. *et al. Nature Physics* (2021).
8. Betti, R. *et al.* Alpha Heating and Burning Plasmas in Inertial Confinement Fusion. *Phys. Rev. Lett.* **114**, 255003 (2015).
9. Nuckolls, J., Wood, L., Thiessen, A. & Zimmerman, G. Laser Compression of Matter to Super-High Densities: Thermonuclear (CTR) Applications. *Nature* **239**, 139–142 (1972).
10. Green, B. *et al.* ITER: burning plasma physics experiment. *Plasma Physics and Controlled Fusion* **45**, 687 (2003).
11. Keilhacker, M. *et al.* High fusion performance from deuterium-tritium plasmas in JET. *Nuclear Fusion* **39**, 209–234 (1999).
12. Atzeni, S. & Meyer-Ter-Vehn, J. *The Physics of Inertial Fusion* (Oxford University Press, Oxford, Great Britain, 2004).
13. Hurricane, O. *et al.* Fuel gain exceeding unity in an inertially confined fusion implosion. *Nature* **506**, 343 (2014).
14. Le Pape, S. *et al.* Fusion Energy Output Greater than the Kinetic Energy of an Imploding Shell at the National Ignition Facility. *Phys. Rev. Lett.* **120**, 245003 (2018).
15. Coppi, B. Evolving Developments for the Scientific Community and for Controlled Nuclear Fusion and Space Research. In B.L. Altshuler, M.A. Vasiliev, L.I. Gurvits, I.M. Dremin, V.I. Ritus, V.E. Fortov, A.E. Shabad (ed.) *Academician A.D. Sakharov. Scientific Works. To His Centenary*, vol. 1 of *Journal of Physics Conference Series* (Fizmatlit Publ., Moscow, 2021, 2021). MIT (LNS) Report HEP 20/03 (2020) to be published in Russian.
16. Moses, E. I. *et al.* The National Ignition Facility: Transition to a User Facility. *Journal of Physics: Conference Series* **688**, 012073 (2016).
17. Lindl, J. Development of the indirect-drive approach to inertial confinement fusion and the target physics basis for ignition and gain. *Phys. Plasmas* **2**, 3933–4024 (1995).
18. Hurricane, O. A. *et al.* Inertially confined fusion plasmas dominated by alpha-particle self-heating. *Nature Physics* **12**, 800 (2016).
19. Casey, D. T. *et al.* The high velocity, high adiabat, "Bigfoot" campaign and tests of indirect-drive implosion scaling. *Phys. Plasmas* **25**, 056308 (2018).
20. Baker, K. L. *et al.* Hotspot parameter scaling with velocity and yield for high-adiabat layered implosions at the National Ignition Facility. *Phys. Rev. E* **102**, 023210 (2020).
21. Callahan, D. A. *et al.* Exploring the limits of case-to-capsule ratio, pulse length, and picket energy for symmetric hohlraum drive on the National Ignition Facility Laser. *Phys. Plasmas* **25**, 056305 (2018).
22. Michel, P. *et al.* Symmetry tuning via controlled crossed-beam energy transfer on the National Ignition Facility. *Phys. Plasmas* **17**, 056305 (2010).
23. Patel, P. K. *et al.* Hotspot conditions achieved in inertial confinement fusion experiments on the National Ignition Facility. *Phys. Plasmas* **27**, 050901 (2020).
24. Landen, O. L. *et al.* Capsule implosion optimization during the indirect-drive National Ignition Campaign. *Phys. Plasmas* **18**, 051002 (2011).
25. Meezan, N. B. *et al.* X-ray driven implosions at ignition relevant velocities on the National Ignition Facility. *Phys. Plasmas* **20**, 056311 (2013).
26. Hurricane, O. *et al.* Physics Principles of Inertial Confinement Fusion (ICF) and Status of the US Program. *Reviews of Modern Physics* **in preparation**, 58 (2021).

27. Lawson, J. D. Some criteria for a power producing thermonuclear reactor. *Proceedings of the Physical Society. Section B* **70**, 6 (1957).
28. Zylstra, A. B. & Hurricane, O. A. On alpha-particle transport in inertial fusion. *Phys. Plasmas* **26**, 062701 (2019).
29. Bosch, H.-S. & Hale, G. Improved formulas for fusion cross-sections and thermal reactivities. *Nuclear Fusion* **32**, 611–631 (1992).
30. Spears, B. K. *et al.* Performance metrics for inertial confinement fusion implosions: Aspects of the technical framework for measuring progress in the National Ignition Campaign. *Phys. Plasmas* **19**, 056316 (2012).
31. Rinderknecht, H. G. *et al.* Azimuthal Drive Asymmetry in Inertial Confinement Fusion Implosions on the National Ignition Facility. *Phys. Rev. Lett.* **124**, 145002 (2020).
32. Tommasini, R. *et al.* Time-Resolved Fuel Density Profiles of the Stagnation Phase of Indirect-Drive Inertial Confinement Implosions. *Phys. Rev. Lett.* **125**, 155003 (2020).
33. Casey, D. T. *et al.* Evidence of Three-Dimensional Asymmetries Seeded by High-Density Carbon-Ablator Nonuniformity in Experiments at the National Ignition Facility. *Phys. Rev. Lett.* **126**, 025002 (2021).
34. Pak, A. *et al.* Impact of Localized Radiative Loss on Inertial Confinement Fusion Implosions. *Phys. Rev. Lett.* **124**, 145001 (2020).
35. Amendt, P. *et al.* Ultra-high ($> 30\%$) coupling efficiency designs for demonstrating central hot-spot ignition on the National Ignition Facility using a Frustraum. *Phys. Plasmas* **26**, 082707 (2019).
36. Landen, O. *et al.* Yield and compression trends and reproducibility at NIF*. *High Energy Density Physics* **36**, 100755 (2020).
37. Cerjan, C., Springer, P. T. & Sepke, S. M. Integrated diagnostic analysis of inertial confinement fusion capsule performance. *Phys. Plasmas* **20**, 056319 (2013).
38. Hurricane, O. A. *et al.* On the importance of minimizing "coast-time" in x-ray driven inertially confined fusion implosions. *Phys. Plasmas* **24**, 092706 (2017).
39. Hurricane, O. A. *et al.* An analytic asymmetric-piston model for the impact of mode-1 shell asymmetry on ICF implosions. *Phys. Plasmas* **27**, 062704 (2020).
40. de Souza, R. S., Boston, S. R., Coc, A. & Iliadis, C. Thermonuclear fusion rates for tritium + deuterium using Bayesian methods. *Phys. Rev. C* **99**, 014619 (2019).
41. Abadi, M. *et al.* Tensorflow: A system for large-scale machine learning. In *12th {USENIX} symposium on operating systems design and implementation ({OSDI} 16)*, 265–283 (2016).

Acknowledgements and Disclaimer We thank Bruno Coppi (MIT), Steven C. Cowley (PPPL), and Dennis Whyte (MIT) for thoughtful discussions. The contributions of NIF operations and target fabrication teams to the success of these experiments are gratefully acknowledged. This work was performed under the auspices of the U.S. Department of Energy by Lawrence Livermore National Laboratory under Contract DE-AC52-07NA27344. This document was prepared as an account of work sponsored by an agency of the United States government. Neither the United States government nor Lawrence Livermore National Security, LLC, nor any of their employees makes any warranty, expressed or implied, or assumes any legal liability or responsibility for the accuracy, completeness, or usefulness of any information, apparatus, product, or process disclosed, or represents that its use would not infringe privately owned rights. Reference herein to any specific commercial product, process, or service by trade name, trademark, manufacturer, or otherwise does not necessarily constitute or imply its endorsement, recommendation, or favoring by the United States government or Lawrence Livermore National Security, LLC. The views and opinions of authors expressed herein do not necessarily state or reflect those of the United States government or Lawrence Livermore National Security, LLC, and shall not be used for advertising or product endorsement purposes. LLNL-JRNL-819741-DRAFT

Author Contributions

A.B.Z. hot-spot analysis lead, Hybrid-E experimental lead, and wrote sections of paper; O.A.H. capsule scale/burning plasma strategy, theory, 0D hot-spot models, and wrote sections of paper; D.A.C. empirical hohlraum P2 model and hohlraum strategy; A.L.K. Hybrid-E design lead, integrated design physics, P2 CBET playbook; J.R. N201101 & N210207 experimentalist and 'Shot RI' (shot responsible individual); H.R. original I-Raum design lead; J.S.R. I-Raum experimental lead and N201122 Shot RI; C.Y. present I-Raum design lead; K.B. Hybrid Shot RI; D.C. Hybrid Shot RI; T.D. Hybrid Shot RI; L.D. 3D hot-spot analysis; M.H. Hybrid Shot RI; S.L.P. Hybrid Shot RI; A.P. Hybrid & I-Raum Shot RI, physics of capsule engineering defects; P.P. 1D hot-spot analysis, Yamp and GLC inference; R.T. Hybrid Shot RI; S.A. capsule microstructure physics; B.B. penumbral x-ray diagnostic; R.B. x-ray framing camera; D.B. LPI physics; R.B. ICF physics/ignition theory; S.B. cryo layering; R.B. RTNAD nuclear diagnostic; N.B. neutron diagnostics; E.B. project engineering; D.B. diagnostics; T.B. capsule fab & metrology; T.B. cryo layering; M.B. project engineering; H.C. GLEH x-ray diagnostic; P.C. DT EOS measurements; T.C. LPI physics; C.C. target fab planning; A.C. ignition theory; D.C. capsule/instability physics; E.D. experiments; J.-M.D.N. MOR and PAM stability, SSD improvements, and FC control; T.D. capsule physics; M.J.E. program management; M.F. target fabrication; J.F. 2DConA image analysis; D.F. nuclear diagnostics; J.F. magnetic recoil spectrometer nuclear diagnostic; J.G. ensemble simulations; G.G. nuclear diagnostics; S.H. capsule physics, iPOM analysis; K.H. neutron diagnostics; G.H. experiments; J.H. power balance analysis; E.H. nuclear time-of-flight diagnostics; J.H. MOR and PAM stability, SSD improvements, and FC control; V.H. MOR and PAM stability, SSD improvements, and FC control; H.H. gamma diagnostics; M.H. program management; D.H. hohlraum physics, CBET studies in Hybrid-C; J.H. x-ray diagnostics; L.B.H. HDC implosion design; W.H. management; K.H. ensemble simulations; N.I. x-ray diagnostics; J.J. neutron diagnostics; M.G.J. magnetic recoil spectrometer diagnostic; O.J. hohlraum physics; S.K. neutron diagnostics; S.K. x-ray diagnostics and analysis; J.K. diagnostic management; Y.K. gamma diagnostics; H.G.K. gamma diagnostics; V.G.K. neutron diagnostics; J.K. hohlraum physics/diagnostic planning; J.K. targets; C.K. capsules O.L.L. velocity analysis; D.L. NIF facility management; N.C.L. optical diagnostics; J.L. ICF physics; A.M. diagnostic management; B.M.G. mode-1 analysis, backscatter; S.M. integrated design physics; A.M. x-ray diagnostics; D.M. x-ray diagnostics; E.M. x-ray diagnostics; L.M. capsule physics; K.M. gamma diagnostics; N.M. hohlraum physics; P.M. LPI physics; M.M. optical diagnostics; J.M. hohlraum physics; J.M. hohlraum physics; A.M. neutron diagnostics; K.N. project engineering; A.N. target fab engineering, capsule, and fab planning; R.N. ensembles simulations; L.P. MOR and PAM stability, SSD improvements, and FC control; L.P. ensembles simulations; N.R. capsules; H.R. RTNAD mode-1 analysis; M.R. hohlraum physics; M.R. x-ray diagnostics; J.S. hohlraum physics; J.S. mode-1 analysis; D.S. neutron diagnostics; M.S. hohlraum diagnostics; K.S. mode-1 metrology; S.S. sagometer data & particle analysis; V.S. capsule physics; B.S. ensemble simulations; P.S. dynamic model, ignition theory; M.S. capsules; S.S. x-ray diagnostics; D.S. hohlraum/LPI physics; C.T. Bigfoot design physics; E.T. optical diagnostics; R.T. program management; C.W. capsule/instability physics; K.W. x-ray diagnostics; C.W. capsule fabrication; C.W. neutron diagnostics; T.W. hohlraum physics; B.W. project engineering; B.V.W. NIF operations lead; P.V. neutron imaging diagnostics; and S.Y. MOR and PAM stability, SSD improvements, and FC control.

Competing Interests The authors declare that they have no competing financial interests.

Correspondence Correspondence and requests for materials should be addressed to O.A.H. and A.B.Z. (emails: hurricane1@llnl.gov, zylstra1@llnl.gov).

1 Methods

Inferred hot-spot conditions Hot-spot conditions must be inferred from measured quantities using a model. The simplest hot-spot model is to assume an isobaric volume of uniform conditions, as used in Ref. 13 between Eq. 2 and 3, in which case the hot spot number density is given by

$$n = 1.2 \times 10^6 \sqrt{\frac{Y}{\langle \sigma v \rangle V_{hs} \tau}} \tag{6}$$

where Y is the fusion yield in J, $\langle \sigma v \rangle$ is the fusion reactivity with depends on the ion temperature (T_i), V_{hs} is the hot-spot volume in cm^3, and τ is the burn duration in s, for equimolar DT mixtures. The remaining hot-spot quantities follow from the inferred density, including the pressure ($P = (1+Z)nk_BT_i$ with Boltzmann's constant), hot-spot energy ($E_{hs} = 1.5PV_{hs}$), and areal density $\left(\rho R = (2.5n/N_a)\sqrt[3]{3V_{hs}/4\pi}\right)$.

A more detailed inference is to use a one-dimensional profile in radius for temperature and density, maintaining the isobaric assumption. A conduction-limited profile follows the expression[37],

$$T(r) = T_{min} + (T_0 - T_{min}) \left[1 - \left(\frac{r}{R_0}\right)^2\right]^{\frac{1}{1+\beta}}, \tag{7}$$

where T_{min} is the temperature at the boundary, T_0 is the central temperature, and R_0 is the hot-spot boundary. β is the thermal conductivity power law, 2.5 from classical Spitzer conductivity. Following Ref. 23 we use a lower value $\beta = 2/3$ which accounts for additional physics, dynamical processes, and reproduces radiation-hydrodynamics simulations. The density profile is then determined by the isobaric assumption through $P \propto nT$ being constant. T_{min} is taken as 1 keV leaving T_0, R_0, and P as free parameters in the model; the data are compared to synthetic data calculated from this 1-D profile with the model parameters adjusted to minimize residuals. As in the 0-D model, the hot-spot energy simply follows from pressure and volume while the areal density is the mass density integrated over the inferred radial profile.

Implosion velocity (v_{imp}) is inferred using a rocket model of the implosion[38] constrained by both supporting experiments, especially in-flight radiography, and the measured time of peak nuclear production on each experiment. The inferred yield amplification given in Table 1 is a function of the measured yield, shell compression, and fuel mass (m_{fuel}); both the velocity and Y_{amp} inferences use the prescription given in Ref. 23. The fuel kinetic energy then follows from $\frac{1}{2} m_{fuel} v_{imp}^2$. Our techniques for inferring the PdV work done on the fuel are discussed in the following section.

A comparison of inferred values using 0-D and 1-D models are shown in Table 2. Inferred pressures are highly consistent between these calculations, while hot-spot energies and areal densities are higher in the 1-D model due to significant mass near the 1keV temperature cutoff.

Inferring G_{fuel} An expression for the fuel gain is given in Eq. 1. The yield is measured and the hot-spot energy is inferred as described in the prior section. Precisely determining the cold-fuel energy from data is not straightforward. For the purposes of this analysis we actually require the total PdV work done on all the DT. This is at least the fuel kinetic energy and internal energy at peak velocity, which are both inferred. The inflowing remaining ablator material can also do work on the fuel, in which case the hot-spot energy is more than half the previous estimate; in this scenario we assume equipartition between the hot spot and cold fuel to evaluate Eq. 1.

Inferred PdV work The primary uncertainty in the Betti metric[8] is in the inference of PdV work on the hot spot, here we use three methodologies: two inferences using an analytic model, and a direct extraction of PdV work from simulations that match the experimental observables.

We use the hydrodynamic piston model of an implosion described in Ref. 39. This analytic model abstracts the implosion process using opposed pistons to represent the imploding shell. In spherical geometry, the stagnation pressure from this mechanical work on the hot spot is given by (Eq. 24 in Ref. 39):

$$P_{piston} = \frac{\rho \delta R_{ave}\, v_{imp}^2}{R_{hs}} (1 - f^2), \tag{8}$$

where $\rho\delta R_{ave}$ is the average shell areal density, calculated from the measured neutron 'down scattered ratio' (DSR) using the relation $\rho\delta R_{ave} \sim 19.3 DSR$, v_{imp} is the implosion velocity, and R_{hs} is the average hot spot radius (which can be obtained from the volume, V_{hs}, given in Table 1). The factor f^2 represents the effect of mode-1 asymmetry and is a measure of the residual kinetic energy (kinetic energy of that is never converted into internal energy) in the implosion.

From the piston pressure we obtain the hot-spot internal energy (IE) from

$$E_{IE} = \frac{3}{2} P_{piston} V_{hs}. \tag{9}$$

In the absence of α-heating (which adds energy to the hot-spot) and radiative x-ray losses or when α-heating exactly balances x-ray losses, $E_{IE} = E_{PdV,hs}$. For low yield amplification implosions ($Y_{amp} < 1.5$), x-ray losses dominate over α-heating energy gains, so $E_{IE} < E_{PdV,hs}$. For higher yield amplification implosions ($Y_{amp} > 2$), α-heating energy gains start to dominate over x-ray losses, so $E_{IE} > E_{PdV,hs}$. The estimated values for these three shots are given in Table 3 as the piston methodology.

We can also estimate the stagnated fuel mass in a similar fashion using

$$m_{shell} = 4\pi R_{hs}^2 \rho \delta R_{ave}, \tag{10}$$

which allows us to then estimate the total mass that stagnates from $m_{shell} + m_{hs}$, with m_{hs} from the hot-spot inferences described earlier. We then estimate the PdV work from

$$E_{PdV} = 0.73 E_K \frac{m_{shell} + m_{hs}}{m_{fuel}}, \tag{11}$$

where m_{fuel} is the initial fuel mass and E_K is the total kinetic energy. The factor of 0.73 is derived from 1-D simulations in which the imploding mass stagnates efficiently, and we drop the residual kinetic energy factor f^2 since the inferred shell mass does not include non-stagnated material. This estimate leads to smaller estimates of $E_{PdV,hs}$ than the first empirical estimate, and are given in Table 3 as the stagnated mass estimate.

For analysis of previously published campaigns we use the simple relation $E_{PdV,hs} \sim (0.5 - 0.7) E_K (1 - f^2)$, this is easy to evaluate with the available data and the factor $0.5-0.7$ accounts for a wide range of 1-D to 2-D/3-D behavior observed on past shots. For comparison, the proportionality constant inferred from the first methodology (Eq. 9) is 0.58 for N201101 (degraded by a large mode-2 asymmetry that is not well accounted for by the f^2 term), and is 0.72 for N201122.

We also employ radiation-hydrodynamics simulations to estimate the PdV work done on these implosions. The first simulation-based methodology is to use 2-D simulations with degradation mechanisms that match the observed performance, and interrogate the work done upon the mass elements which form the hot spot to infer $E_{PdV,hs}$. The simulation methodology is described in Ref. 6, and the values of $E_{PdV,hs}$ for this method are given in Table 3. The same fusion performance can be generated with varying application of degradation mechanisms that either degrade $E_{PdV,hs}$ or do not; an estimate of the 2-D simulation uncertainty of ± 0.5 kJ is estimated by studying multiple simulations.

A similar energy-balance analysis can be done with 1-D simulations, in which the work done upon the hot spot is well defined with

Table 2 | Comparison of inferred quantities from 0-D and 1-D hot-spot models.

	N201101		N201122		N210207		N210220	
	0-D	1-D	0-D	1-D	0-D	1-D	0-D	1-D
P (GBar)	312^{+37}_{-29}	306^{+35}_{-29}	295^{+21}_{-19}	289^{+21}_{-18}	338^{+27}_{-23}	334^{+27}_{-23}	351^{+50}_{-42}	318^{+43}_{-36}
E_{hs} (kJ)	$11.9^{+1.4}_{-1.1}$	$15.2^{+1.8}_{-1.5}$	$11.3^{+0.8}_{-0.7}$	$14.3^{+1.1}_{-1.0}$	$16.9^{+1.3}_{-1.1}$	$21.3^{+1.8}_{-1.5}$	$13.1^{+1.7}_{-1.5}$	$17.8^{+2.3}_{-2.2}$
ρR_{hs} (g/cm^2)	$0.36^{+0.06}_{-0.04}$	$0.38^{+0.06}_{-0.05}$	$0.33^{+0.04}_{-0.03}$	$0.34^{+0.04}_{-0.03}$	$0.36^{+0.04}_{-0.03}$	$0.38^{+0.04}_{-0.04}$	$0.36^{+0.04}_{-0.03}$	$0.37^{+0.04}_{-0.04}$

Table 3 | Inferred hot-spot PdV work by different methodologies, ordered from smallest to largest estimates.

		N201101	N201122	N210207	N210220
Data	Stag. Mass	8.1 ± 0.9	7.2 ± 0.8	8.5 ± 0.9	6.5 ± 1.1
	Piston	9.5 ± 0.8	8.6 ± 0.7	10.6 ± 0.9	8.5 ± 1.4
Sim.	2-D	10.1 ± 0.5	10.1 ± 0.5	11?	10.5?
	1-D	11.3	10.4	11.1	10.5?

a Lagrangian mesh. The 1-D simulations are tuned to match the measured yields, but are expected to overestimate $E_{PdV,hs}$ since they cannot properly incorporate residual kinetic energy. This estimate is given in Table 3 as an upper bound.

We have thus develop four methodologies for estimating $E_{PdV,hs}$. In the main analysis we use a combination of the empirical piston model estimate as the more pessimistic data-based inference, and use the 2-D simulated $E_{PdV,hs}$ as the most robust computational description of the experiments.

Model uncertainties for Hurricane's metric The Hurricane metric[3] depends on more quantities than the Betti metric, although these quantities are more straightforward to infer than $E_{PdV,hs}$. The metric reduces to (Eq. 9 in Ref. 3):

$$7.4 \times 10^{25} f_\alpha \left(\rho R_{hs}\right) \frac{\langle \sigma v \rangle}{T_i} > v_{imp}, \tag{12}$$

where ρR_{hs} and v_{imp} are inferred as described previously, and T_i is measured. f_α is the alpha-stopping fraction which is model dependent, and $\langle \sigma v \rangle$ contains some systematic uncertainty from the evaluation used.

Data uncertainties are well-defined for T_i and in the inference of ρR_{hs} and v_{imp}, and are propagated as described in the next section; the inferred ρR_{hs} can also vary between models, which will be discussed.

For f_α we used the published fits from Ref. 28, this work used two independent and modern stopping-power theories which agreed well with each other, the primary approximation in Ref. 28 is that a uniform 0-D hot spot profile was used. For more realistic systems, even the 1-D model described previously, the stopping efficacy should increase due to a higher weighting of the fusion reactions towards the center of the hot spot and an increase in stopping power at the edges of the hot spot where the temperature is lower. We therefore consider the f_α values used as a pessimistic estimate for the purposes of evaluating Hurricane's criteria.

Eq. 12 depends on the fusion reactivity; in this work we use the evaluation from Bosch and Hale [29]. Recent publications have presented alternative evaluations[40] which differ by $\sim 2\%$. We note that the inferred $\rho R \propto 1/\sqrt{\langle \sigma v \rangle}$ from Eq. 6, so the condition in Eq. 12 depends on the reactivity as $1/\sqrt{\langle \sigma v \rangle}$. f_α is also weakly increasing with ρR, leading to the condition being slightly less than square-root dependent on $\langle \sigma v \rangle$, so this criteria has $< 1\%$ uncertainty from the choice of $\langle \sigma v \rangle$ evaluation.

The Hurricane criteria is sensitive to the inferred hot-spot ρR, which can vary between models depending on the spatial dependence of ρ. As shown in Table 2, the 0-D and 1-D hot-spot models agree quite well. We also check these values using a 3-D reconstruction of the hot spot density and temperature profiles [a yet unpublished method of L. Divol, but briefly described in 34], for N201101 this gives a value of $\rho R_{hs} \sim 0.36 - 0.38$ g/cm^2 to the 1 keV contour for N201101 and $\rho R_{hs} \sim 0.35 - 0.36$ g/cm^2 for N201122. These values are consistent with the simple models described earlier.

Uncertainty analysis We perform uncertainty analysis for all hot-spot quantities by propagating the normally-distributed uncertainties in measured quantities through the 0-D and 1-D models described earlier. The model input parameters are those that fully describe the system, and are constrained by the measured yield, ion temperature, burn widths (from both x rays and γ rays), and volume from the 17% contour of neutron emissivity. Distributions of model parameters are generated using Markov Chain Monte Carlo (MCMC), calculated with the `tensorflow`[41] probability package. The log-likelihood function for MCMC is defined by the measurements and calculated with the log-likelihood function

$$-\frac{1}{2}\sum_i \left(\frac{m_i - y_i}{\delta y_i}\right)^2, \tag{13}$$

which is summed over all observables (i) where m_i is the model value, y_i is the measured value, and δy_i is the uncertainty in the measurement. This methodology produces full distributions of the model parameters including any correlations, from the model parameter distributions we generate full distributions of all hot-spot parameters, some of which exhibit correlation, such as in the temperature and areal density required to evaluate the Hurricane metric, which are partially anti-correlated (evident in Fig. 3a). Other inferences, such as the implosion velocity or kinetic energy, are treated with normally-distributed uncertainties that are uncorrelated with the hot-spot inferences.

Power balance relations In evaluating the power-balance relations relevant to Eq. 5 we use the following expressions for the individual terms:

$$P_\alpha = 8.2 \times 10^{24} \rho \langle \sigma v \rangle, \tag{14}$$

$$P_b = 3.1 \times 10^{7} \rho \sqrt{T}, \tag{15}$$

$$P_e = 5.9 \times 10^{3} \frac{T^{3.5}}{\rho R^2}. \tag{16}$$

In these expressions the specific powers are given in units of GJ/(g·s) and thus are multiplied by the inferred hot-spot mass to obtain power. ρ is the hot-spot mass in g/cm^3, $\langle \sigma v \rangle$ is the fusion reactivity evaluated as a function of temperature in cm^3/s, T is the temperature in keV, and ρR is the hot-spot areal density in g/cm^2. The self-heating power P_α is multiplied by the fraction of alpha-particle energy deposited in the hot spot (f_α) using the evaluation published in Ref. 28. For all three shots $f_\alpha \sim 0.77 - 0.80$.